Materials and Design 31 (2010) 3463–3473

Contents lists available at ScienceDirect

Materials and Design

journal homepage: www.elsevier.com/locate/matdes

Design-optimization and material selection for a femoral-fracture fixation-plate implant

M. Grujicic [a,*], G. Arakere [a], X. Xie [a], M. LaBerge [b], A. Grujicic [b], D.W. Wagner [c], A. Vallejo [c]

[a] Department of Mechanical Engineering, Clemson University, Clemson, SC 29634-0921, United States
[b] Department of Bioengineering, Clemson University, Clemson, SC 29634, United States
[c] Ozen Engineering, Inc., 1210 E. Arques Avenue, Suite: 207, Sunnyvale, CA 94085, United States

ARTICLE INFO

Article history:
Received 17 July 2009
Accepted 20 January 2010
Available online 25 January 2010

Keywords:
Musculoskeletal modeling and simulations
Femoral-fracture fixed-plate implant
Optimization

ABSTRACT

The problem of size/thickness optimization of a distal femoral-fracture fixation-plate is addressed computationally using a combined finite-element/design-optimization procedure. To obtain realistic physiological loading conditions associated with normal living activities (cycling, in the present case), a musculoskeletal multi-body inverse-dynamics analysis is carried out of a human riding the bicycle. While optimizing the design of the femoral-fracture locking-plate, realistic functional requirements pertaining to attain the required level of fracture-femur fixation and longevity/lifecycle were used. It is argued that these types of analysis should be used to complement pre-clinical implant-evaluation tests, the tests which normally include a limited number of physiological loading conditions and single pass/fail outcomes/decisions with respect to a set of lower-bound implant–performance criteria.

1. Introduction

Significant advantages are associated with the use of internal fracture fixation devices to repair broken long bones such as the femur, humerus, and tibia. Beside decreasing the bone healing time and allowing for a more accurate anatomical axial alignment, the patient can return to activities of daily leaving more rapidly [1]. The failure of fracture fixation devices is attributed to biological factors such as extensive soft-tissue traumatic injury, atrophic fracture site, and dead space among others [1]. From a mechanical perspective, the strength of the device and its ability to sustain dynamic loading associated with activities of daily living have been identified as critical factors to predict performance [2]. Pre-clinical implant evaluation studies performed to estimate their mechanical performance suffer from at least two major shortcomings: (a) they rely on a limited number of physiological loading conditions; and (b) the results of these studies are used only to determine if the implant has passed or failed a set of minimum-level performance criteria [3–5].

Consequently, redesign of new implants is carried out only when the design has failed to meet these criteria. What is left unanswered is if the accepted new implant can meet the performance and longevity requirements under other physiological loading conditions associated with normal daily living and if the design (including the material selected for the implant) are optimal (with respect to their size, weight, cost, etc.).

The main objective of the present work is to demonstrate how musculoskeletal modeling can be used to determine physiological loading conditions not normally covered by pre-clinical implant-evaluation tests although they may refer to fairly normal daily activities (e.g. cycling). Within the present work, the recently-developed novel technology for computer modeling of the human-body mechanics and dynamics, namely the AnyBody Modeling System [6] and its associated public domain library of body models are being fully utilized and further developed. In its most recent rendition [7], the AnyBody Modeling System enables creation of a detailed computer model for the human body (including all important components of the musculo-skeletal system) as well as examination of the influence of different postures and the environment on the internal joint forces and muscle activity.

The second main objective of the present paper is to demonstrate how the loading conditions derived using musculoskeletal modeling can be utilized within a combined finite-element/design-optimization procedure to carry out optimization of the design of an implanted device. Specifically, optimal thickness of a distal femoral-fracture fixation-plate under pedaling (cycling) exertion loading conditions is investigated. Optimization of the implant design/thickness is carried out with respect to its ability to meet several functional requirements pertaining to both the necessary level of fractured-femur fixation and to meeting the longevity/lifespan constraints. Details regarding these functional requirements are presented in the next section.

* Corresponding author. Address: 241 Engineering Innovation Building, Clemson University, Clemson, SC 29634-0921, United States. Tel.: +1 864 656 5639; fax: +1 864 656 4435.
E-mail address: mica.grujicic@ces.clemson.edu (M. Grujicic).

0261-3069/$ - see front matter © 2010 Elsevier Ltd. All rights reserved.
doi:10.1016/j.matdes.2010.01.036

The organization of the paper is as follows. A brief overview of the AnyBody Modeling System is provided in Section 2.1. The musculoskeletal human-body model, the concepts of muscle recruitment and muscle-activity envelope, the bicycle model and the issues related to human/bicycle kinematics and contact interactions are discussed in Sections 2.2–2.5. The definition of the musculoskeletal problem of a human riding the bicycle analyzed in the present work is discussed in Section 2.6. The finite-element/design-optimization problem and analysis for the distal femoral-fracture fixed-plate implant are presented in Section 3. The results obtained in the present work are presented and discussed in Section 4. The main conclusions resulting from the present work are summarized in Section 5.

2. Musculoskeletal modeling and simulation

As mentioned earlier, two distinct computational analyses are carried out in the present work. Within the first analysis (discussed in this section), a musculoskeletal investigation of a person riding a bicycle is carried out. The resulting forces and moments, as a function of time, acting on the fractured right femur of the person riding the bicycle are next used in a finite-element/design-optimization analysis of the distal femoral-fracture fixation-plate implant.

2.1. The AnyBody Modeling System [6]

The AnyBody Modeling System [6] developed at Aalborg University and used in the present work is a general-purpose musculoskeletal modeling and simulation program. The essential features of this computer program can be summarized as follows:

(a) The musculoskeletal model is typically constructed as a standard multi-body dynamics model consisting of rigid bodies, kinematic joints, kinematic drivers and force/moment actuators (i.e. muscles). The kinematic and dynamic behavior of this model can be determined using standard multi-body dynamics simulation methods;
(b) Complex geometries of the muscles and their spatial arrangement/interactions (e.g. muscles wrapping around other muscles, bones, ligaments, etc.) can be readily modeled within AnyBody Modeling System [6];
(c) It is well-established that a typical musculo-skeletal system suffers from the so-called *"muscle redundancy problem"*: i.e. the number of muscles available is generally larger than those needed to drive various body joints. Within the living humans and animals, this problem is handled by their Central Nervous System (CNS) which controls muscles activation/recruitment. To mimic this role of the CNS, the AnyBody Modeling System [6] offers the choice of several optimization-based muscle-recruitment criteria;
(d) A typical musculoskeletal multi-body dynamics problem is solved using computationally-efficient inverse dynamics methods within which the desired motion is prescribed while the muscle activity required to produce this motion is computed;
(e) Within the AnyBody Modeling System [6], the muscle recruitment problem is solved using an optimization-based approach in the form:

Minimize the objective function:

$$G(f^{(M)}) \tag{1}$$

Subjected to the following constraints:

$$Cf = d \tag{2}$$

$$f_i^{(M)} \geqslant 0, \quad i \in \{1, \ldots, n^{(M)}\} \tag{3}$$

where the objective function G (a scalar function of the vector of $n^{(M)}$ unknown muscle forces, $f^{(M)}$), defines the minimization object of the selected muscle-recruitment criterion (assumed to mimic the one used by the CNS). Eq. (2) defines the condition for dynamic mechanical equilibrium where C is the coefficient matrix for the "*unknown*" forces/moments in the system while d is a vector of the "*known*" (applied or inertia) forces. The forces appearing in vector f in Eq. (2) include the unknown muscle forces, $f^{(M)}$, and the joint-reaction forces, $f^{(R)}$. Eq. (3) simply states that muscles can only pull (not push) and that the upper bound for the force in each muscle $f_i^{(M)}{}_i$ is the corresponding muscle strength, N_i;

(f) While there are a number of functional forms for the objective function, G, the one used in the present work is the so-called "*min/max*" form within which the objective function (to be minimized) is defined as the maximum muscle activity defined for each muscle i as $f_i^{(M)}/N_i$, i.e.:

$$G(f^{(M)}) = \max\,(f_i^{(M)}/N_i) \tag{4}$$

This formulation offers several numerical advantages over other popular forms of G and, in addition, it appears to be physiologically sound. That is, under the assumption that muscle fatigue is directly proportional to its activity, Eqs. (1) and (4) essentially state that muscle recruitment is based on a minimum muscle-fatigue criterion. Also, this expression for G, has been found to asymptotically approach other formulations of G (e.g. the so-called "*Polynomial*" form [8]).

(g) The problem defined by Eqs. ((1)–(4)) can be linearized using the so-called "*bound formulation*" [9] resulting in a linear programming problem with muscle forces and joint-reaction forces as free variables. Relations between these two types of forces are next used to eliminate the joint-reaction forces yielding a linear programming problem with the number of unknowns equal to the number of muscles in the system; and
(h) While for a fairly detailed full-body model containing around one thousand muscles, this constitutes a medium-to-large size problem which can be readily solved by a variety of design-optimization methods (e.g. Simplex, Interior-point methods, etc.), the min/max problem is inherently indeterminate and must be solved iteratively. This can be rationalized as follows: The min/max criterion only deals with the maximally-activated muscles and with muscles which help support the maximally-activated muscles. Since the system, in general, may contain muscles that have no influence on the maximum muscle activity in the system, the forces in these muscles are left undetermined by the min/max formulation presented above. To overcome this shortcoming, the muscle-recruitment optimization problem is solved iteratively, so that each iteration eliminates the muscles with uniquely determined forces and the procedure is repeated until all muscle forces are determined.

2.2. Musculoskeletal human-body model

The musculoskeletal model of the human body used in the present work was downloaded from the public domain AnyScript Model Repository [10]. The model was originally constructed by

AnyBody Technology using the AnyBody Modeling System [6] following the procedure described in details by Damsgaard et al. [7].

Model Taxonomy: The musculoskeletal human-body model includes: (a) an arm/shoulder assembly containing 114 muscle units on each side of the body and having a morphology defined by Van der Helm [11], (b) a spine model developed by de Zee et al. [12] comprising sacrum, all lumbar vertebrae, a rigid thoracic-spine section, and a total of 158 muscles, and (c) a pelvis and lower extremity model with a total of 70 muscles. In total, the model contains more than 500 individual muscle units and, hence, can be considered as a fairly detailed description of the human musculo-skeletal system. The anthropometrical dimensions of the model are selected in such a way that they correspond to the female cyclist participated in the motion-capture tests, Section 2.7.

2.2.1. Segments and joints

Within the model, the bodies (referred to as the "segments" within the AnyBody Modeling System) are treated as rigid with their mass/inertia properties derived from mass and shape of the associated bone and the soft tissue that is allotted to the bone. Joints in the human body are treated as idealized frictionless kinematic constraints between the adjoining segments. Both standard kinematic joints (e.g. spherical joints for the hips, hinge joints for the knees, etc.) as well as specially-developed joints (e.g. those used to represent kinematic constraints associated with floating of the scapula on the thorax) are employed.

2.2.2. Muscles

Muscles are treated as string contractile force–activation elements which span the distance between the origin and the insertion points through either the via points or by wrapping over the surfaces which stand on their way. Muscle wrapping problem is treated using a shortest-path contact-mechanics algorithm. Due to the fact that the problem considered in the present work is dynamic, muscles are modeled as being non-isometric (i.e. muscle strength is considered to be a function of the body posture and the rate of contraction). Also, passive elasticity of muscles (i.e. the resistance of the muscles to stretching) was considered.

2.2.3. Model validations

The mechanics of the model is implemented as a full three-dimensional Cartesian formulation and includes inertial and gravity body forces. Integral validation of whole-body musculoskeletal models is very difficult to conduct. To the best knowledge of the present authors, validation of the whole-body musculoskeletal model is still lacking (due to major challenges which would be associated with such validation). However, various subsystems of the whole-body model were validated separately. For e.g.: (a) The lumbar spine model was validated by de Zee et al. [12] by comparing the model prediction with in vivo L4–5 intradiscal pressure measurements of Wilke et al. [13]; (b) de Jong et al. [14] validated the lower extremity model by comparing model-predicted muscle activations and pedal forces with their experimental counterparts obtained in pedaling experiments; and (c) The shoulder model was validated in the early work of Van der Helm [11].

2.3. The muscle-activity envelope

As originally recognized by An et al. [15], the min/max muscle-recruitment formulation, discussed in Section 2.1, defines effectively a minimum fatigue criterion as the basis for muscle recruitment, i.e. the aim of the proposed muscle-recruitment strategy is to postpone fatigue of the "hardest-working" muscle(s) as far as possible. The physiological consequence of this strategy is that muscles tend to form groups with muscles within the same group having comparable activity levels. In particular, in the muscle group associated with the maximum muscle activity there will be usually many muscles which, in a coordinated manner, carry a portion of the load comparable with their individual strengths. Consequently, in this group, many muscles will have the same activity level, which will be referred to as "the muscle-activity envelope". The linearity of the reformulated min/max criterion discussed earlier guarantees that the optimization problem defined by Eqs. ((1)–(3)), is convex and, hence, that the solution to the problem is unique and corresponds to the global optimum. In other words, there is no other muscle-recruitment strategy which can reduce the muscle-activity envelope further. Moreover, since the muscle-activity envelope represents the maximum muscle activation in the model, it can be interpreted as the fraction of maximum voluntary contraction necessary to support the imposed load (gravity and inertia forces, in the present case) while maintaining the prescribed posture. Thus, the muscle-activity envelope appears to be an important parameter/measure for ergonomic-design optimization, in the sense that designs which are associated with lower envelope levels may be perceived as less fatigue-inducing.

2.4. Bicycle model

The raised-frame-bicycle used in the present musculoskeletal cycling analysis was comprised of four segments: a frame, a crank and two wheels. Three revolute joints are used to connect the crank and the two wheels to the frame.

The effort that the human body must exert in order to drive the bicycle was modeled by prescribing a time-dependent resistance crank torque. The mean value of this torque was computed using an average value of the cycling power of 170 W. The torque amplitude was defined by subtracting from the mean torque the so-called "*dead-center crank torque*" (a value of the torque the cyclist must provide when the pedal arms are close to the vertical position and when the tangential pedal-force direction is nearly perpendicular to the preferred force direction of the legs). To comply with the fact that the two pedals function equally the crank-torque frequency is set to twice the cadence value.

2.5. Human-body/bicycle kinematics and interactions

The interactions between the cyclist and the bicycle were handled as follows: (a) two spherical joints were used to connect the human hands to the bicycle-frame/handle-bar. These connections were attained through the use of gloves (one per each hand). Gloves are special elements in AnyBody which enable the definition of the joints with a finite strength and, thus, can be used to emulate the grip strength of a normal hand. This typically eliminates numerical problems (i.e. unreasonable results) associated with the use of infinitely-strong human-body/environment joints; (b) the feet are connected to the peddle/crank using a pair of revolute joints; and (c) a general purpose joint based on linear and rotational measures was defined between the pelvis and the bicycle saddle/seat.

To quantify the extent of and to account for the distributed nature of the human-body/bicycle-seat contact interactions, a number of support points are introduced over the bicycle-saddle surface. These support points allow the transfer of reaction forces to the bicycle-seat via the so-called "*support elements*". These elements enable quantification of the human-body/bicycle-seat contact (compressive and tangential/friction) reaction forces at the support points. It should be noted that the compressive reaction forces are perpendicular to the support surfaces while tangential force can be in any direction perpendicular to the corresponding compressive force.

Due to the presence of the aforementioned human-body/bicycle kinematic links, the human body acquires the appropriate posture

for each angular position of the bicycle-crank. In the process of acquiring the appropriate posture, kinematics of the spine is adjusted in accordance with the so-called "spinal rhythm" algorithm. Within this algorithm, a single input, the pelvis-thorax angle, is used to determine the three rotational-joint angles of adjacent vertebrae (under a condition that the passive-elastic elements of the spine are able to force the spine to act kinematically as an elastic beam). The physical soundness of the spinal-rhythm algorithm for the seating posture has been validated by Rasmussen and de Zee using motion capture experiments [16].

In acquiring the sought posture for the human, an additional algorithm was employed. This algorithm controls the relative magnitudes of hip flexion and pelvis/thorax flexion. Following the experiments of Bell and Stigant [17], the ratio of the two angles was set to 2. That is, for a given value of the angle between the thorax and the thigh, the hip-joint flexion angle is twice that of the spine flexion angle.

2.6. Musculoskeletal definition of the cycling problem

To position the human body (overviewed in Section 2.3) onto the bicycle and have it drive the bicycle, laboratory experiments were conducted. Within these experiments, an experienced cyclist was instrumented with reflective markers on the outside of her thighs, knees, and ankles, Fig. 1. After a bicycle specialist adjusted a raised-frame bicycle to match the anthropometry of the bicycle rider, the cyclist was asked to cycle at a comfortable speed (corresponding to the average cadence of 62 rpm). Meanwhile, motion capture measurements were carried out in order to locate and track the position of the reflective markers. The marker-position data recorded as a function of time were then used as input to the AnyBody Modeling System to drive the human-body model during cycling, Fig. 2.

3. Finite-element and design-optimization procedures

As mentioned earlier, the results of the musculoskeletal cycling analysis in the form of muscle forces and femur/hip and femur/knee joint-reaction forces and moments, along with the spatial coordinates of the muscle attachment/via points and the two joints (as a function of time), are exported from the AnyBody Modeling System and used, as input, in a finite-element/design-optimization analysis of the distal femoral-fracture fixation-plate implant, Some details pertaining to the finite-element/design-optimization analysis are presented in the remainder of this section. In Fig. 3, the names and the spatial locations of the muscle-attachment/via points and the hip and knee joints are provided for the right femur. In this figure, there are 27 muscle attachment/via points and two joint points. Moments are transferred to the femur only at the two joint points since muscles, being contractile linear elements, can each provide only a force.

Fig. 1. Participant in the raised-frame-bicycle motion-capture experiments.

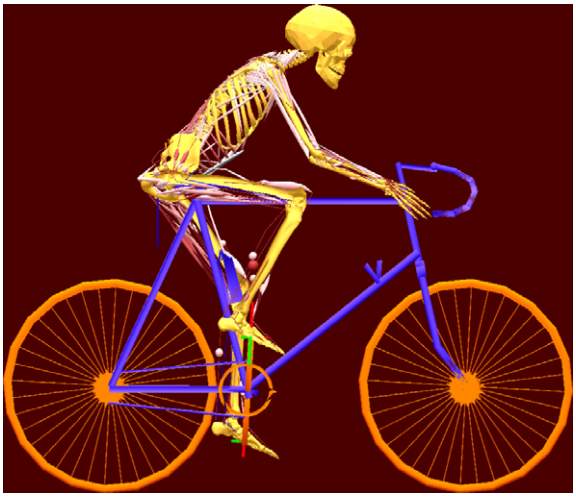

Fig. 2. Scaled musculoskeletal model of a person riding a bicycle (not scaled to size).

In Fig. 4, a close-up is provided of the right femur along with the adjoining bones. As can be seen, the femur contains a distal (next to the knee) fracture and it is fixed with a lateral fracture fixation-plate implant. The implant is attached to the two segments of the fractured femur using seven screws.

3.1. Finite-element model and analysis

3.1.1. The model

The finite-element model analyzed consisted of a fractured right femur, a fixation-plate implant and seven locking screws. Typical finite-element meshes used are displayed in Fig. 5. The femur, the plate and each of the screws were discretized using ca. 24,000 tetrahedral solid elements, ca. 9000 tetrahedral solid elements and ca. 7000 hexahedral solid elements, respectively.

To apply the muscle forces and joint-reaction forces and moments to the femur, each muscle-attachment/joint point is combined with a neighboring section of the femur surface to form a coupling. In this way, forces/moments acting at a muscle-attachment/joint point are transferred to the femur over a larger surface area preventing (unrealistic) stress-concentration artifacts.

To fasten the screws to the fixation plate and to the two bone segments, the outer surfaces of the screws are tied to the mating surfaces of the plate/femur. In other words, perfect fastening is assumed to have been achieved using the screws.

To prevent sections of the bottom surface of the fixation-plate implant between the screws from penetrating the femur, a "*penalty-type*" contact algorithm was employed. Within this algorithm, penetration of the contacting surfaces is opposed by a set of contact springs. Any level of contact pressure can be transmitted through the contact interface. Shear stresses are transmitted across the contact-interface in accordance with the Coulomb friction law.

3.1.2. Material models

The fixation-plate implant and the seven screws are assumed to be made of Ti–6Al–4 V, a Ti-based alloy which is commonly used in

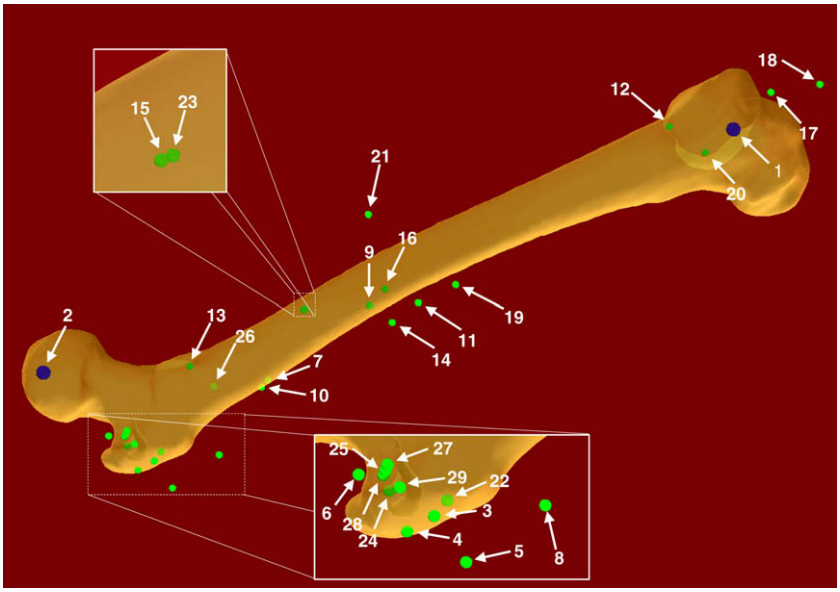

1 - Knee Joint Reference Node
2 - Hip Joint Reference Node
3 - Gluteus Minimus Node
4 - Gluteus Medius Node
5 - Gluteus Maximus1 via Node 2
6 - Gluteus Maximus2 via Node3
7 - Gluteus Maximus3 Node
8 - Tensor Fasciae Latae via Node2
9 - Adductor Longus Node
10 - Adductor Magnus1 Node
11 - Adductor Magnus2 Node
12 - Adductor Magnus3 Node
13 - Iliopsoas Node
14 - Vastus Lateralis Node
15 - Vastus Medialis Node
16 - Vastus Intermedius Node
17 - Quadriceps via Node1
18 - Quadriceps via Node2
19 - Biceps Femoris Caput Breve Node
20 - Gastrocnemius Node
21 - Sartorius via Node1
22 - Quadratus Femoris Node
23 - Abductor Brevis Node
24 - Obturatorius Externus Node
25 - Obturatorius Internus Node
26 - Pectineus Node
27 - Gemellus Superior Node
28 - Gemellus Inferior Node
29 - Piriformis Node

Fig. 3. Spatial location of various muscle attachment points to the right femur.

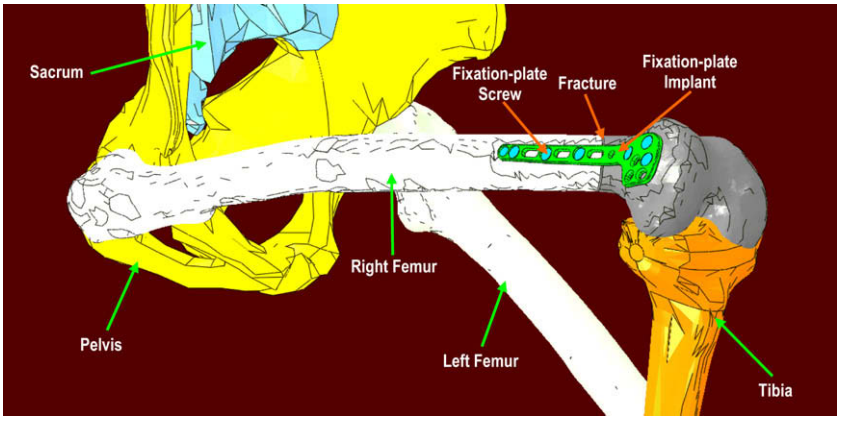

Fig. 4. A close-up view of the fractured right femur (with a lateral fixation-plate implant and locking screws) and the adjoining bones at one time instant during a cycling-simulation run.

fractured-bone fixation applications. Ti–6Al–4 V is modeled as a linear-elastic/ideal-plastic material.

To provide a higher level of realism to the analysis, it is recognized that femur is built of two types of bone tissues (*cortical* and *trabecular*) and that density (and hence mechanical properties) of the two types of bone tissues are spatially non-uniform. To obtain the necessary data for defining the cortical-bone/trabecular-bone dividing surfaces and the spatial distribution of the density within each of the two bone tissues, computed tomography (CT) scans of the femur bone were analyzed [18]. An example of the CT scan of the femur bone is shown in Fig. 6. For each bone tissue, the local gray-scale level is proportional to the local density. CT images like the one displayed in Fig. 6 are analyzed using the Medical Imaging Software Mimics [19]. Within Mimics, the two bone tissues are differentiated by assigning two non-overlapping gray-scale ranges, one for each bone tissue. Then, the gray-scale of each pixel within the two bone tissues is quantified using the Hounsfield Unit (HU) value. The latter are next converted into the corresponding bone-density values as: $\rho = 1.9\,\mathrm{HU}/1700$, where the bone-density ρ is given in g/cm^3. Lastly, the relations listed in Ta-

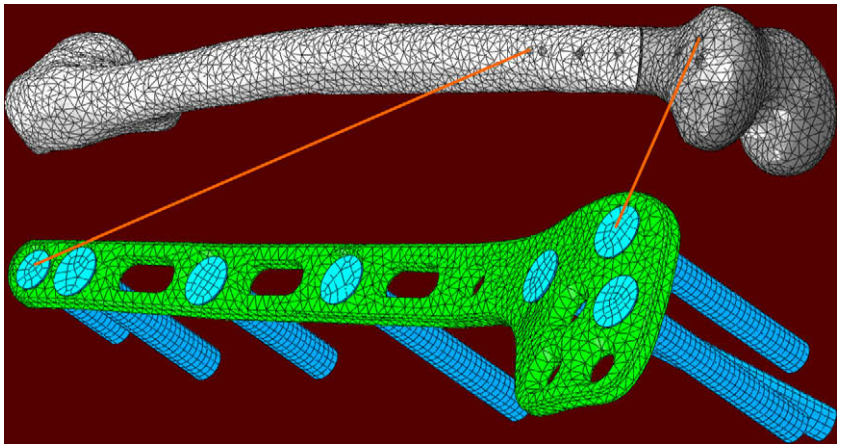

Fig. 5. Typical finite-element meshes for the femur, fixation-plate implant and seven screws used in the quasi-static analysis of the implant longevity.

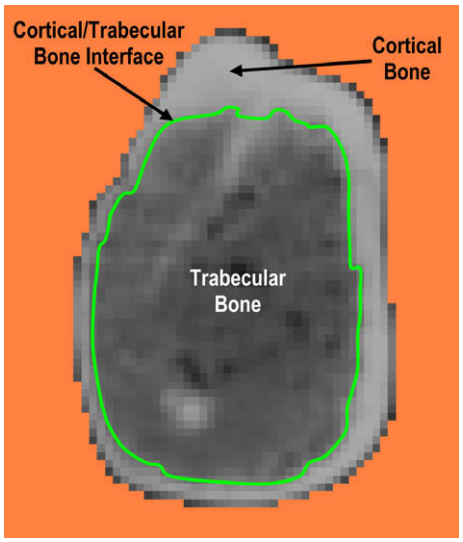

Fig. 6. A typical computed tomography (CT) scan of the femur showing the presence of two bone tissues (cortical and trabecular bone tissues) and density variation within each bone-tissue.

ble 1 in [18] were used to compute the Young's modulus as a function of the local density within the two bone tissues. A constant value of $v = 0.3$ was used for both bone tissues. No plasticity within the femur was considered. In other words, it was assumed that the femur was made of two isotropic heterogeneous linear-elastic materials.

3.1.3. The analysis

The results of the AnyBody-based multi-body dynamic cycling analysis over a single revolution of the bicycle crank are exported at 100 equal time intervals. For each of these intervals, a quasi-static finite-element analysis of the femur/fixation-plate/screws assembly is carried out. At each of these time steps, the following AnyBody output information was used. (a) Spatial position of the femur/fixation-plate/screw assembly and the associated muscle-attachment and joint-reaction points; (b) muscle forces and joint-reaction forces and moments; and (c) the femur/plate/screws assembly (linear and angular) velocities and accelerations.

The aforementioned AnyBody output data were used within the finite-element model as follows: (a) the spatial position data were used to correctly position the finite-element model and the points for the application of concentrated forces and moments; (b) The muscle-force and joint-reaction force/moment data were used to define concentrated-load type of boundary conditions; and (c) the velocity and acceleration data were used to define distributed (gravity, inertia and centripetal) loading conditions.

The finite-element analysis results were used to determine: (a) if the fixation – plate implant has suffered (unacceptable) plastic deformation; (b) if the two contacting fractured surfaces of the femur have intruded into each other (also an unacceptable scenario); and (c) if the stress-state of the most critical elements (elements which control the fatigue life of the fixation-plate implant).

All the calculations pertaining to the quasi-static response of the femur/plate/screws assembly are done using ABAQUS/Standard, a commercially available general-purpose finite-element program [20].

3.2. Design-optimization analysis

One of the main objectives of the present work was to carry out optimization of the femoral-fracture fixation-plate implant design. For simplicity, the overall implant-design was assumed to remain fixed except for the plate thickness. Since the plate was modeled as a solid structure, changes in its thickness entailed re-meshing of this component during optimization. In addition, since the screws length also changed during optimization to comply with the plate thickness, the screws had to be remeshed as well. In other words, while only the fixation-plate thickness was being altered, the optimization procedure was essentially a shape rather than a size based optimization.

Table 1
Functional relations used to compute, from CT-scans, density and the Young's modulus in the cortical and trabecular bones of the radius.

Bone region	Density (ρ) vs. hounsfield unit (HU) relationship	Young's modulus (E) vs. density (ρ) relationship
Cortical bone	$\rho\ (\mathrm{g/cm^3}) = 1.9\frac{HU}{1700}$	$E\ (\mathrm{MPa}) = -13{,}430 + 1426\rho(\mathrm{g/cm^3})$
Trabecular bone	$\rho\ (\mathrm{g/cm^3}) = 1.9\frac{HU}{1700}$	$E\ (\mathrm{MPa}) = 1310(\rho(\mathrm{g/cm^3}))^{1.40}$

3.2.1. Structural optimization

Structural optimization is a class of engineering optimization problems in which the evaluation of an objective function(s) or constraints requires the use of structural analyzes (typically a finite-element analysis, *FEA*). In compact form, the optimization problem can be symbolically defined as [21]:

Minimize the objective function $f(x)$.
Subjected to the non-equality constraints $g(x) < 0$ and
to the equality constraints $h(x) = 0$.
with the design variables x belonging to the domain D.

where in general, $g(x)$ and $h(x)$ are vector functions. The design variables x form a vector of parameters describing the geometry of a part/component. For e.g., x, $f(x)$, $g(x)$ and $h(x)$ can be part dimensions, part weight, a stress condition defining the onset of plastic yielding, and constraints on part dimensions, respectively. Depending on the nature of design variable in question, its domain D can be continuous, discrete or a mixture of the two. Furthermore, a structural optimization may have multiple objectives, in which case the objective function becomes a vector function.

Structural optimizations can be classified in many different ways. One of these classifications distinguishes between topology, size and shape optimization methods.

3.2.1.1. Topology optimization. Topology optimization which is typically applied at the conceptual stage of part design represents the design domain as the continuum mixture of a solid material and "*voids*" and the optimal design is defined with respect to the distributions of the mixture density within the design space [22].

3.2.1.2. Size optimization. Within size optimization approach, the dimensions that describe part geometry are used as design variables, x. The application of size optimization is, consequently, mostly used at the detailed part-design stage where only fine tuning of the part geometry is necessary. Size optimization is typically quite straightforward and it generally requires no re-meshing of the finite-element models during optimization iterations.

3.2.1.3. Shape optimization. Shape optimization which is also mostly used at the detailed part-design stage, allows the changes in the boundary of part geometry. The boundaries are typically represented as smooth parametric curves/surfaces, since irregular boundaries typically deteriorate the accuracy of finite-element analysis or may even cause the numerical instability of optimization algorithms. Because the product geometry can change dramatically during the optimization process, the automatic re-meshing of finite-element models is usually required. Structural shape optimization methods are generally classified as: (a) direct geometry manipulation and (b) indirect geometry manipulation approaches. In the direct geometry manipulation approaches, design variable x is a vector of parameters representing the geometry of part boundary, e.g., the control points of the boundary surfaces. In the indirect geometry manipulation approaches, design variable x is a vector of parameters that indirectly defines the boundary of the product geometry. A comprehensive review of shape optimization based on the direct and the indirect geometry manipulation approaches can be found in Ref. [23].

3.2.2. Fixation-plate shape optimization

The fixation-plate thickness optimization problem was defined as follows: The plate thickness is to be minimized while ensuring that during cycling no plastic deformation in the plate takes place, no interpenetration of the two fractured-femur segments occur and that no high-cycle fatigue failure will take place after a pre-selected number of bicycle-crank revolutions (two million cycles, in accordance with a simple analysis presented in Section 4). Due to the three-dimensional nature of the fixation-plate implant, its thickness optimization was handled as a shape-optimization problem. Eight shape variables were used, one for the plate and the remaining ones for each of the seven screws of the fixation-plate. Each shape variable enables a proportional change in the geometry of the associated component while ensuring a high-quality of their finite-element mesh. This was accomplished by using mesh-morphing algorithm which preserves identity of the nodes and elements while simply repositioning the nodes. The fixation-plate thickness-optimization problem was implemented into and solved using HyperStudy [24], a general purpose multi-disciplinary multi-objective optimization software. For a defined optimization problem, this software invokes the pre-selected optimization algorithm (the Adaptive Response Surface Method [25], in the present case), morphs the component meshes, prepares an input file for the finite-element analysis, launches the finite-element solver and reads and interprets the finite-element results in order to determine the immediate direction of the design-optimization process.

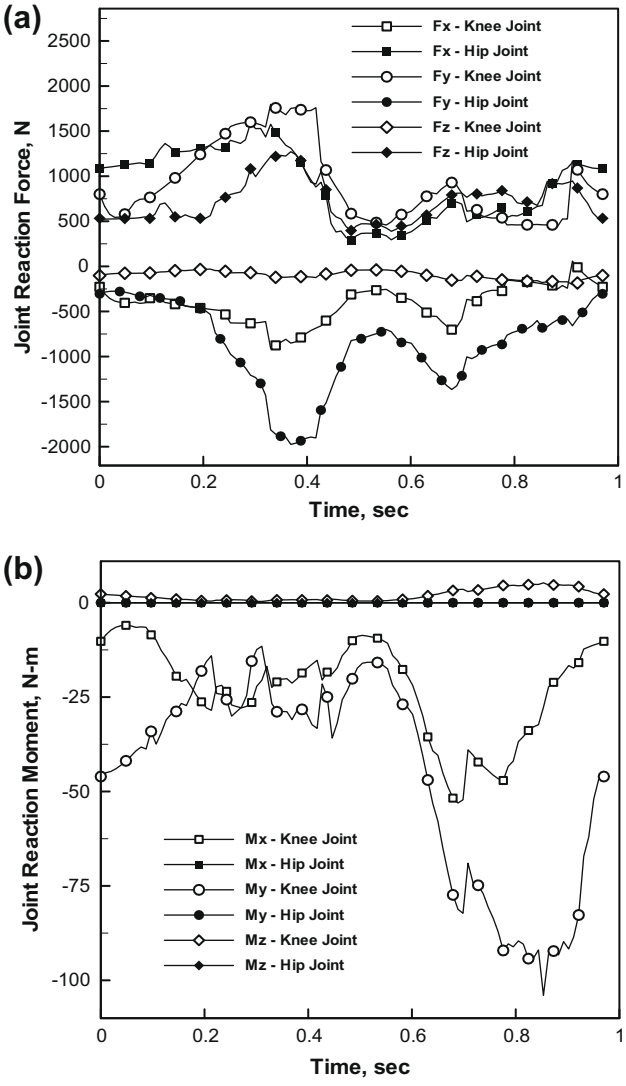

Fig. 7. Temporal evolution of the hip and knee joint-reaction forces and moments over a single revolution of the bicycle crank.

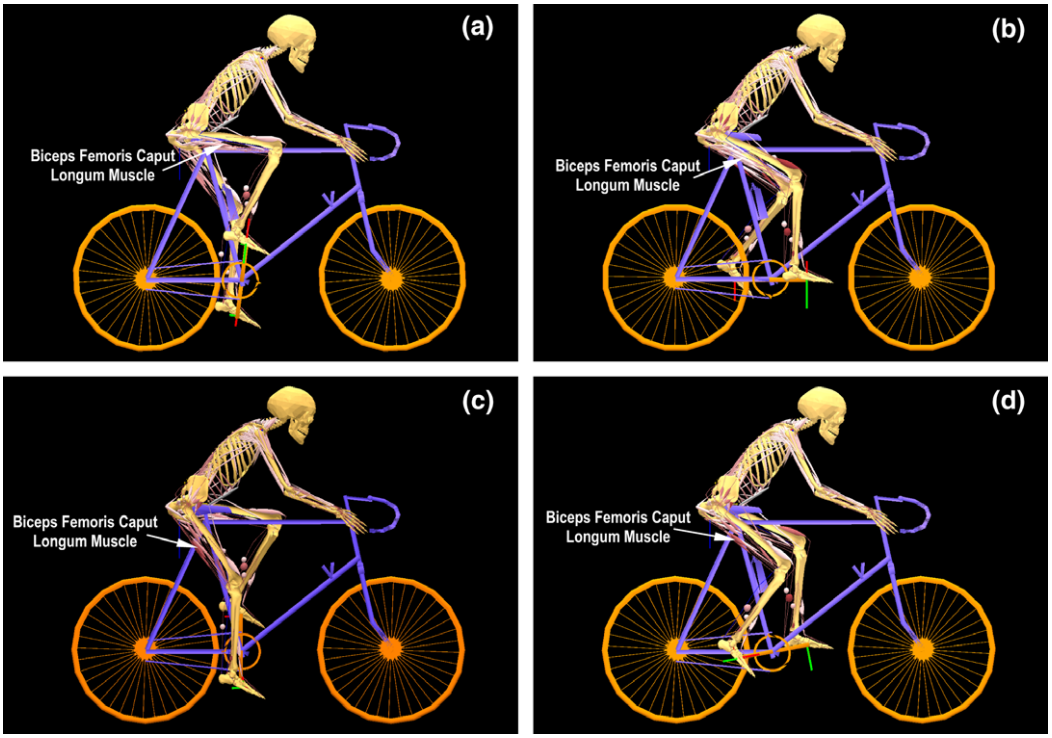

Fig. 8. Temporal evolution of the human-body kinematics and muscles activity at four equally-spaced times during a single bicycle-crank revolution.

3.2.3. Fatigue-life prediction

As mentioned earlier, one of the fixation-plate design-optimization constraints pertains to the attainment of a pre-selected lifecycle. Since this lifecycle is expected to be high-cycle fatigue controlled, a fatigue-based lifecycle prediction procedure had to be developed in the present work. The first step in this direction was to examine the temporal behavior of the muscle forces and reaction forces and moments during a single revolution of the bicycle crank. An example of the results obtained for the two joint-reaction force and moment components is displayed in Fig. 7a and b. Simple examination of the results displayed in these figures show that the temporal evolution of various forces and moments is not in-phase and that these forces/moments are not associated with constant amplitude. These findings have important consequences to the type of fatigue-life prediction analysis which should be employed. Firstly, the non-constant nature of the load amplitude implies that a cycle-counting procedure (e.g. the so-called *Rainflow cycle-counting analysis* [26]) should be employed in order to represent (highly-irregular) time-dependent loading as a collection of constant-amplitude (fixed mean-value) loading cycles. Secondly, since temporal evolution of the various muscle forces and joint-reaction forces and moments are out of phase, not only the magnitude of stresses/strains at an arbitrary point in the femur/plate/screw assembly varies as a function of time, but also the orientation of the associated principal coordinate system is time variant. The latter findings are what makes the loading "*non-proportional*" and the fatigue-life prediction more complex. Specifically, the rainflow cycle-counting analysis to be used should differentiate the load cycles not only on the basis of their amplitude and the mean value but also on the basis of the orientation of their stress/strain principal coordinate system.

3.2.4. High-cycle stress-based fatigue analysis

Due to a relatively simple geometry of the fixation-plate implant and the fact that a pre-defined high-cycle fatigue life is mandated for this component, it was deemed reasonable to assume that the fatigue-life of this component will be stress controlled. Furthermore it is assumed that the stress-based function responsible for the fatigue-induced failure is the maximum principal (tensile) stress. Next, stress-amplitude dependence of the number of cycles till failure is assumed to be defined by the traditional Basquin relation [27] and the effect of the mean value of the maximum principal (tensile) stress is accounted for through the use of Goodman relation [27]. The high-cycle fatigue parameters for Ti–6Al–4 V are obtained from the Ansys fatigue material database [28].

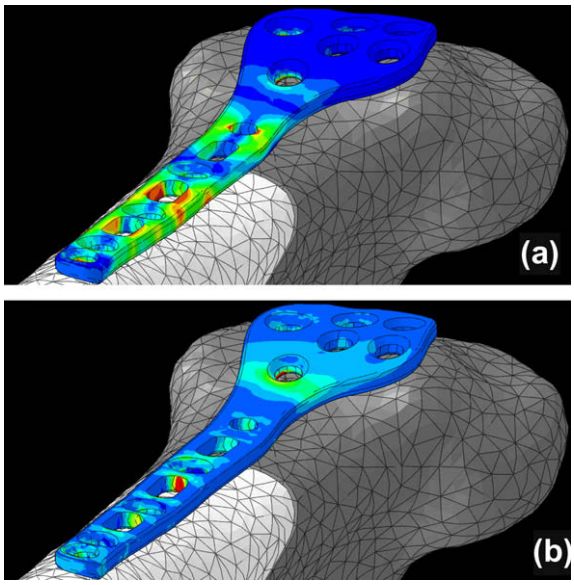

Fig. 9. Typical results pertaining to the spatial distribution of: (a) von-Mises equivalent stress (red = 30 MPa and blue = 0.1 MPa) and (b) maximum principal stress (red = 20 MPa and blue = −3 MPa). (For interpretation of the references to colour in this figure legend, the reader is referred to the web version of this article.)

To compute the number of cycles till failure for the given design/thickness of the fixation-plate implant, the procedure developed in our previous work was utilized [29]. Due to space limitations, only a brief overview of this procedure will be provided here. The main steps of this procedure applied to each finite element of the fixation-plate implant include: (a) utilization of the finite-element calculation results to determine temporal evolution of the maximum principal (tensile) stress; (b) application of the rainflow cycle-counting analysis to determine a three dimensional histogram relating the number of cycles with the maximum principal stress amplitude and the associated mean value; (c) calculation of the fractional damage associated with each load-cycle type (as characterized by a fixed value of the stress amplitude and the stress mean value); and (d) computation of the total fractional damage associated with all load-cycle types and computation of the corresponding number of cycles till failure as an inverse of this fractional damage.

The fixation-plate implant life cycle is then set to that of its element associated with the smallest number of cycle till failure.

4. Results and discussion

4.1. Musculoskeletal cycling analysis

As mentioned earlier the sole purpose of conducting the musculoskeletal cycling analysis was to obtain physiologically realistic loading conditions for the femur/fixation-plate/screws assembly. Specifically, at each of 100 times increment during a single rotation of the bicycle crank, the muscle forces and the joint-reaction forces and moments as well as the spatial position of the muscle attachment/via points and the joint-reaction points had to be obtained from the musculoskeletal analysis. In addition, the spatial position and the orientation of the femur/plate/screws assembly at each time increment had to be obtained from the musculoskeletal analysis.

An example of the temporal evolution of the forces and moments acting on the femur (at the hip and knee joint points) was shown earlier, Fig. 7a and b. Similar results were obtained at muscle attachment/via points. As pointed out earlier these forces and moments are of non-constant amplitude and not in-phase resulting in non-proportional type of loading on the femur.

An example of the whole human-body/bicycle kinematics/muscle-activity results at four time intervals during a single revolution of the bicycle crank is shown in Fig. 8a–d. It should be noted that the activity of each muscle (i.e. the force produced by the muscle) is displayed pictorially in these figures by the thickness and the color shading of the line segments representing the muscles. The results displayed in Fig. 8a–d then can be used to qualitatively assess how the activity/recruitment of different muscles is changing during a single revolution of the bicycle crank for e.g., variation in the activity of the *Biceps Femoris Caput Longum* muscle is marked in these figures.

4.2. Finite-element results

Since it was assumed throughout this work that the locking screws can secure well the fixation-plate implant to the two fractured-femur segments, the focus of the finite-element investigation was placed on the fixation-plate implant. The three primary functional requirements imposed onto the implant were: (a) sufficiently high strength to prevent any plastic deformation within the fixation plate; (b) adequate bending stiffness to prevent the two femur segments from intruding into each other; and (c) a pre-selected fatigue life expressed as a number of bicycle-crank revolutions. Using an expected implant resident time of 6 years and an average cycling distance of 1000 km/year the implant fatigue life was set to two million cycles.

An example of the typical finite-element results is displayed in Fig. 9a and b. The results shown in Fig. 9a show that the von-Mises equivalent stress is substantially lower than the Ti–6Al–4 V yield strength (930 MPa). Thus under all the loading and fixation-plate design conditions the implant strength requirement was found to be met. Likewise, the conditions regarding the maximum interpenetration of the fracture surfaces of the femur was found to be satisfied (i.e.<0.001 m) for all combinations of loading conditions and the fixation-plate thickness. As far as the fixation-plate implant fatigue-life requirements is concerned, it is found to be satisfied at the implant-thickness upper-bound (4.25 mm) and not to be satisfied at the implant thickness lower-bound (3.25 mm). As mentioned earlier the fatigue-life in the present case is controlled by the maximum principal stress. Fig. 9b displays an example of the typical results pertaining to spatial distribution of this stress component. Clearly the elements surrounding some of the screw-holes are associated with the highest levels of the maximum principal stress and are likely to control the overall fatigue-life of the component.

4.3. Design optimization results

As stated earlier, under all the implant-design and muscle/joint-imposed loading conditions, the functional requirements for the implant pertaining to its strength and bending stiffness were found to be satisfied. Hence, they will not be considered any further. The focus will be placed in this section on the functional requirement pertaining to the fatigue-life of the implant.

In accordance with the discussion presented in Section 3.2, the implant-thickness optimization problem was treated as a shape-design optimization problem. The implant thickness was defined

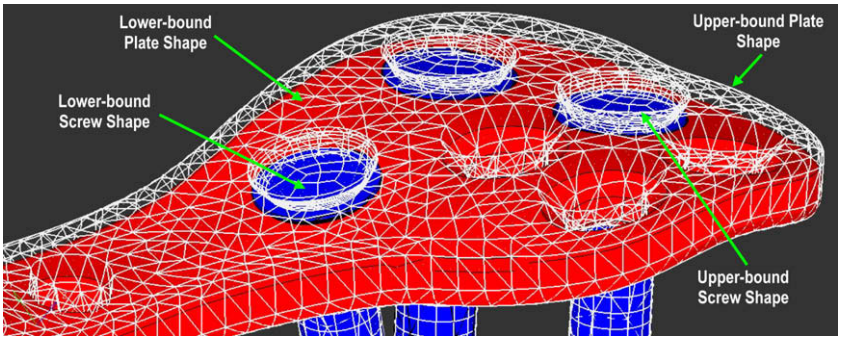

Fig. 10. Upper-bound (wireframe) and lower-bound (shaded red for the plate and blue for the locking screws) shapes used in the fixation-plate thickness design-optimization analysis. (For interpretation of the references to colour in this figure legend, the reader is referred to the web version of this article.)

as a single implant-shape variable. Definition of this shape variable is depicted in Fig. 10. Additionally, the corresponding seven shape variables were defined (only three shown for brevity), one for each locking screw, in order to ensure that screws length is consistent with the implant thickness.

The progress of the implant-thickness optimization is displayed in Fig. 11a and b. In Fig. 11a, implant thickness is tracked as a function of the iteration number. In Fig. 11b, on the other hand, the implant fatigue life is monitored as a function of the optimization iteration number. The results displayed in Fig. 11a and b show that the optimal thickness of the fractured-femur fixation-plate implant is around 4.07 mm.

4.4. Material selection

Until this point in the present investigation, the same implant material, Ti–6Al–4 V STA (*Solution Treated and Aged*) alloy was used. This is a commonly used fractured-femur fixation-plate implant material which provides a good combination of bio-compatibility, mechanical performance and a low material/manufacturing cost. The present investigation has established that the key performance aspect of the fixation-plate implant under consideration is fatigue life. While retaining the requirements concerning low material/manufacturing cost and bio-compatibility (ensured by carrying out material selection within the family of Ti-based alloys), a material selection procedure was conducted in the present work in order to identify potential material substitutes for Ti–6Al–4 V.

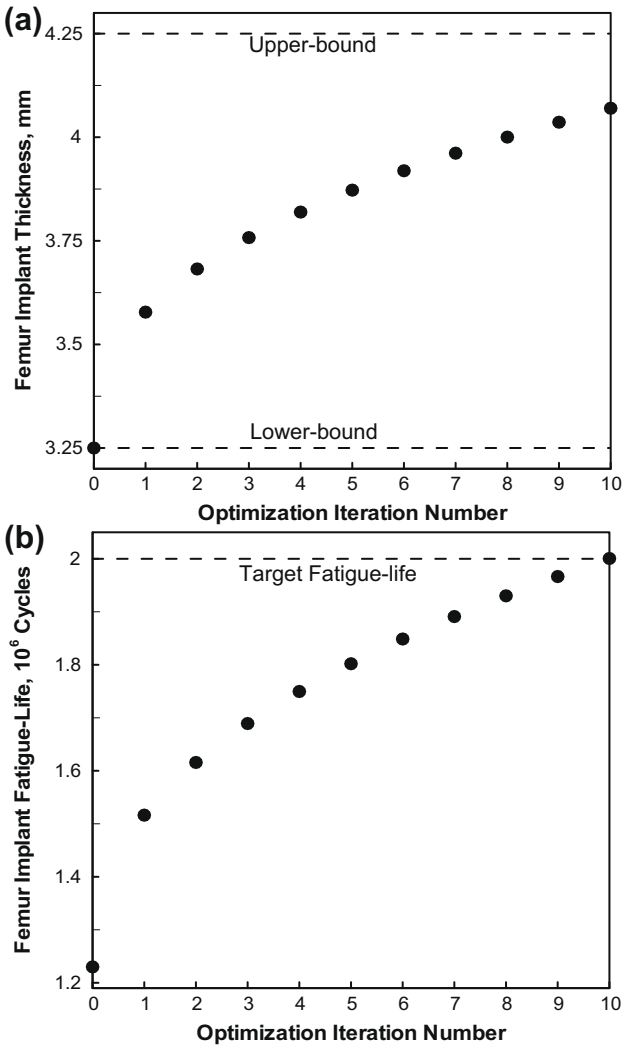

Fig. 11. Variations of: (a) the femur fixation-plate implant thickness and (b) femur implant fatigue-life, with the successive design-optimization iteration numbers.

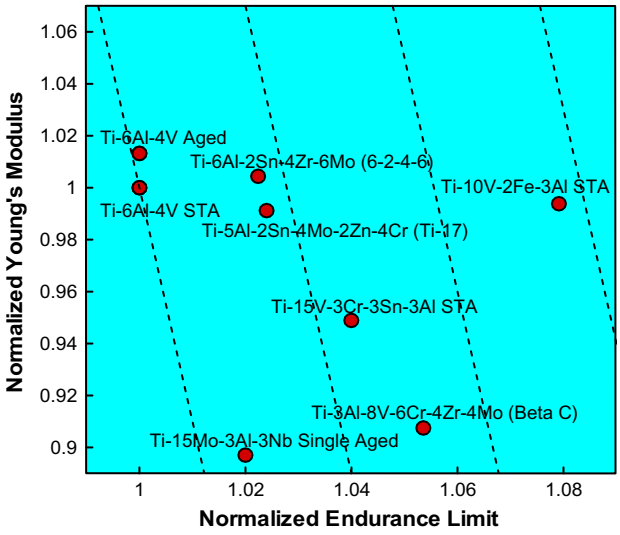

Fig. 12. Material selection chart used in the analysis of potential replacement of Ti–6Al–4 V as the fixation-plate implant material with other Ti-based alloys.

While examining different Ti-based material alternatives, it was found that in all cases considered, strength requirement can be readily attained. Consequently, implant-material selection is carried out with respect to simultaneously, satisfying the implant stiffness and longevity requirements. In all the cases considered, it was found that the longevity requirement is more difficult to meet. Consequently, in defining a single material selection parameter, a higher weighting factor ($w_{EL} = 0.8$) was selected for endurance limit and a lower weighting factor ($w_{YM} = 0.2$) for the Young's modulus of the candidate material. For convenience, the endurance limit and then Young's modulus of each candidate material are normalized by their respective counterparts in Ti–6Al–4 V. Thus, the material selection index for the fixation-plate implant is defined as:

$$M = w_{EL}\frac{\sigma_{EL}}{\sigma_{EL,Ti-6Al-4V}} + w_{YM}\frac{E}{E_{Ti-6Al-4V}} \tag{5}$$

where σ_{EL} denotes endurance limit while E is Young's modulus.

Clearly, $M = 1.0$ for Ti–6Al–4 V and for a material to be considered as a potential substitute for Ti–6Al–4 V, its M must be larger than 1.0.

To assist the implant material-selection process, a normalized stiffness ($E/E_{Ti-6Al-4V}$) vs. normalized endurance limit ($\sigma/\sigma_{Ti-6Al-4V}$) plot is constructed in Fig. 12. Few iso-M lines are also drawn in this figure. The results displayed in Fig. 12 show that, with respect to the implant performance (as defined by its strength, stiffness, and longevity), Ti–10 V–2Fe–3Al STA, Ti–3Al–8 V–6Cr–4Zr–4Mo (Beta C) or Ti–15 V–3Cr–3Sn–3Al STA may be a better alternative for the implant than Ti–6Al–4 V. However, the final decision regarding the substitution of Ti–6Al–4 V with these material alternatives should also account for material/manufacturing cost. Due to a lack of reliable/stable data pertaining to the cost of the materials in question, the effect of cost on material selection could not be taken into account in the present work.

5. Summary and conclusions

Based on the work conducted and the results obtained in the present investigation, the following main summary remarks and conclusions can be drawn:

1. Design (more specifically thickness) optimization of a fractured-femur fixation-plate implant is investigated computationally. To provide the realistic physiological loading conditions experienced by the implant during normal daily activities of the patient, a musculoskeletal multi-body dynamics analysis is coupled with implant finite-element/design-optimization methods.
2. The results show that out of the three functional requirements placed on the implant, (i.e. its strength, bending stiffness and longevity), it is longevity which typically controls the implant optimal design/thickness.
3. Under the assumption that bicycle riding provides the most critical loading conditions experienced by the femur-fixation implant during normal daily activities of the human with a surgically implanted femur-fixation plate, the optimal implant thickness was determined.
4. Potential material replacements have been considered for Ti–6Al–4 V, the alloy used in the present finite-element/design-optimization analysis of a femur-fixation implant, in order to further reduce implant thickness.

Acknowledgements

A portion of the material presented in this paper is based on the use of the AnyBody Modeling System, a musculoskeletal multi-body dynamics software [6]. The authors are indebted to Ozen Engineering for donating an AnyBody Modeling System license to Clemson University. One of the authors (G.A.) would like to acknowledge the support of Altair engineering under the Altair University Fellowship program.

References

[1] Rozbruch SR, Müller U, Gautier E, Ganz R. The evolution of femoral shaft plating technique. Clin Orthop Relat Res 1998;354:195–208.
[2] Pappas CA, Young PG, Lee AJ. Controlled plastic deformation for the fastening mechanism of an internal fixation device-the new mennen 3 peripro plate. Comput Methods Biomech Biomed Eng 2007;10(2):111–20.
[3] Zickel RE. Fractures of the adult femur excluding the femoral head and neck: a review and evaluation of current therapy. Clin Orthop Relat Res 1980;147:93–114.
[4] Otto RJ, Moed BR, Bledsoe JG. Biomechanical comparison of polyaxial-type locking plates and a fixed-angle locking plate for internal fixation of distal femur fractures. J Orthop Trauma 2009;23(9):645–52.
[5] Cegoñino J, García Aznar JM, Doblaré M, Palanca D, Seral B, Seral FA. Comparative analysis of different treatments for distal femur fractures using the finite element method. Comput Methods Biomech Biomed Eng 2004;7(5):245–56.
[6] AnyBody 3.0, Aalborg, Denmark, AnyBody Technology A/S; 2008.
[7] Damsgaard M, Rasmussen J, Christensen ST, Surma E, de Zee M. Analysis of musculoskeletal systems in the anybody modeling system. Simul Model Pract Theory 2006;14:1100–11.
[8] Rasmussen J, de Zee M. Design optimization of airline seats. In: SAE conference, SAE No. 2008-01-1863; 2008.
[9] Dendorfer S, Torholm S. Final report on feasibility study. Report No.: 21385/08/NL/PA, presented to ESTEC/ESA by AnyBody Technology A/S; May 2008.
[10] AnyScript model repository 7.1. AnyBody 3.0, Aalborg, Denmark, AnyBody Technology A/S; 2009.
[11] Van der Helm FCT. A finite element musculoskeletal model of the human shoulder mechanism. J Biomech 1994;27:551–69.
[12] de Zee M, Hansen L, Wong C, Rasmussen J, Simonsen EB. A generic detailed rigid-body lumbar spine model. J Biomech 2007;40:1219–27.
[13] Wilke H, Neef P, Hinz B, Seidel H, Claes L. Intradiscal pressure together with anthropometric data – a data set for the validation of models. Clin Biomech 2001;16(Suppl. 1):S111–26.
[14] de Jong P., de Zee M, Hilbers PAJ, Savelberg HHCM, van de Vosse FN, Wagemakers A, et al. Multi-body modeling of recumbent cycling: an optimization of configuration and cadence. Master's Thesis. Medical engineering, TU/e biomodelling and bioinformatics, University of Maastricht, Movement Sciences, Aalborg University; 2006.
[15] An KN, Kwak BM, Chao EY, Morrey BF. Determination of muscle and joint forces: a new technique to solve the indeterminate problem. J Biomech Eng 1984;106:364–7.
[16] Rasmussen J, Torholm S, de Zee M. Computational analysis of the influence of seat pan inclination and friction on muscle activity and spinal joint forces. Int J Indus Ergon 2009;39:52–7.
[17] Bell JA, Stigant M. Development of a fibre optic goniometer system to measure lumbar and hip movement to detect activities and their lumbar postures. J Med Eng Technol 2007;31:361–6.
[18] Yosibash Z, Padan R, Joscowicz L, Milgrom C. A CT-based high-order finite element analysis of the human proximal femur compared to in-vitro experiments. ASME J Biomech Eng 2007;129(3):297–309.
[19] Mimics. Medical imaging software, Materialise, user documentation; 2009
[20] ABAQUS Version 6.8-1. User documentation. Dassault Systems; 2009.
[21] Papalambros PY, Wilde DJ. Principles of optimal design: modeling and computation. 2nd ed. Cambridge (UK): Cambridge University Press; 2000.
[22] Bendsoe MP, Kikuchi N. Generating optimal topologies in structural design using a homogenization method. Comput Methods Appl Mech Eng 1988;71(2):197–224.
[23] Haftka RT, Grandhi RV. Structural shape optimization: a survey. Comput Methods Appl Mech Eng 1986;57(1):91–106.
[24] HyperStudy. User Manual. Troy (MI), Altair Engineering Inc.; 2009.
[25] Schramm U. Multi-disciplinary optimization for NVH and crashworthiness. Troy (MI), Altair Engineering Inc.; 2007.
[26] Matsuishi M, Endo T. Fatigue of metals subjected to varying stress, In: Proceedings of Kyushi Branch; 1987.
[27] Brondsted P, Lilholt H, Lystrup A. Composite materials for wind power turbine blades. Annual Rev Mater Res 2005;35:505–38.
[28] ANSYS Version 12. User documentation. Ansys Inc.; 2009.
[29] Grujicic M, Arakere G, Bell WC, Marvi H, Yalavarthy HV, Pandurangan B, Haque I, Fadel GM. Reliability-based design optimization for durability of ground-vehicle suspension-system components. J Mater Eng Perform, 2009.